ACS APPLIED MATERIALS & INTERFACES

Research Article

www.acsami.org

Fabrication of Nanocapsule Carriers from Multilayer-Coated Vaterite Calcium Carbonate Nanoparticles

Aniket Biswas,[†] Ashvin T. Nagaraja,[†] and Michael J. McShane*[,†,‡]

[†]Department of Biomedical Engineering and [‡]Department of Materials Science and Engineering, Texas A&M University, College Station, Texas 77843, United States

Supporting Information

ABSTRACT: Nanosized luminescent sensors were prepared as reagents for optical sensing and imaging of oxygen using ratiometric emission properties of a two-dye system. Polymeric capsules were fabricated utilizing poly(vinylsulfonic acid) (PVSA)-stabilized vaterite $CaCO_3$ nanoparticles (CCNPs) as sacrificial templates. The buffer and polymeric surfactant requirements of the layer-by-layer (LbL) process were evaluated toward deposition of multilayer coatings and, ultimately, formation of hollow capsules using these interesting materials. CCNPs were found to be more stable in alkaline $NaHCO_3$ buffer after repeated cycles of washing under sonication and resuspension. An intermediate PVSA concentration was required to maximize the loading of oxygen-sensitive porphyrin and oxygen-insensitive fluorescent nanoparticles in the CCNPs while maintaining minimal nanoparticle size. The CCNPs were then coated with polyelectrolyte multilayers and subsequent removal of the $CaCO_3$ core yielded nanocapsules containing dye and fluorescent nanoparticles. The resulting nanocapsules with encapsulated luminophores functioned effectively as oxygen sensors with a quenching response of 89.28 ± 2.59%, and O_2 (S = 1/2) = 20.91 μM of dissolved oxygen.

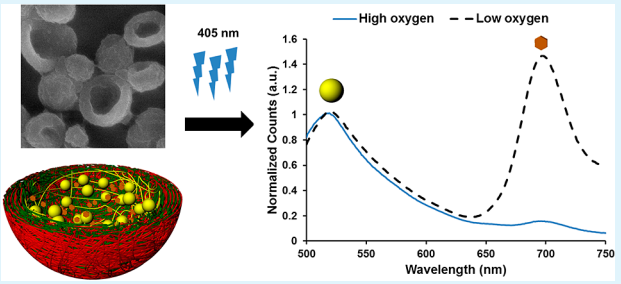

KEYWORDS: *calcium carbonate, phosphorescence, porphyrins, nanocapsules, layer-by-layer self-assembly, vaterite, oxygen sensing*

INTRODUCTION

Microcapsules and nanocapsules have received significant attention for a wide variety of cross-disciplinary applications, e.g., biomedicine, biotechnology, and catalysis.[1] Nanocapsules have advantages over microcapsules when it comes to biosensing and therapeutic drug delivery, including greater cargo encapsulation efficiency[2] and prolonged circulation time, as they can evade processes like phagocytosis and filtration/sequestering in specialized organs.[3,4] Although there is still debate regarding the mechanisms and consistency of this effect, nanosized structures have also been shown in many studies to accumulate in cancerous tissue due to the so-called "enhanced permeability and retention" (EPR) effect.[5] Tumors growing subcutaneously have been shown to have a pore size cut off of 200−1200 nm,[6] making nanocapsules ideal candidates as therapeutic agent carrying containers and for encapsulating sensing chemistry. Tumor cells are typically characterized by hypoxic conditions[7] and abnormal local pH,[8,9] thus sensing pH and oxygen concentration in vivo can serve as potential prognostic/diagnostic tools for cancer.

Approaches to fabricate nanocapsules may be broadly classified as either self-assembly or template-based methods. The self-assembly method makes use of lipid molecules[10] or amphiphilic block copolymers[11] which aggregate into spherical hollow structures in aqueous solution when present at levels above the critical micelle concentration. These hollow aggregates may be used to form stable nanocapsules using various reactions. Unfortunately, nanocapsules made by the self-assembly method are often plagued by issues pertaining to size polydispersity,[12] requiring further research for better control over both the size and morphology and to achieve multi modal versatility.[13] The template-based method requires a particle template around which a polymer shell is fabricated, and subsequent removal of the template generates a hollow polymeric capsule.[14] The template is chosen such that it retains its structural properties during the polymer coating process, while having the capability to easily dissolve after the desired polymer has been attached to its surface. The template-based method may be subdivided into the surface polymerization route and the layer-by-layer (LbL) approach. The surface polymerization method involves surface modification of colloidal particles followed by monomer polymerization on the colloidal seed.[15]

The LbL film fabrication method extensively studied by Decher[16] was utilized by Shukhorukov et al.[17] to make polymeric capsules using colloidal templates. The polymeric shell properties can be tailored to meet specific requirements by changing the type of polyelectrolyte used and by controlling the deposition conditions. Apart from using conventional electrostatic forces of interactions between the cationic/anionic

Received: September 10, 2014
Accepted: November 5, 2014
Published: November 5, 2014

polymers used for the LbL process, forces such as covalent bonding, hydrogen bonding and van der Waals interactions have also been used in the LbL process. The versatility of the LbL process expands the palette from which materials may be selected for the LbL process, which allows for a very broad range of possibilities for capsule properties.[18] The freedom to use a wide range of polyelectrolytes and different fabrication conditions allows fine-tuning of the polymeric capsules properties. The LbL method has been successfully used to fabricate polymeric capsules that are environmentally responsive, capable of biospecific recognition, and resistant to protein fouling.[19] A myriad of materials have also been used as colloidal templates for fabricating polymeric capsules via the LbL approach by various research groups in the past, including popular examples such as melamine formaldehyde,[20] polystyrene,[21] silica,[22] gold,[23] and calcium carbonate.[24]

The semipermeable nature of polymeric capsules can be tuned by the LbL approach to confine the sensor chemistry macromolecules to the capsule interior while allowing small analyte molecules to permeate freely.[25] The possibility of entrapping multiple analyte-sensitive fluorophores/reference dyes simultaneously make them ideal candidates for use as multimodal sensors and ratiometric sensors. The use of LbL capsules as chemical and biosensors was first described in the early 2000s.[26−29] These initial demonstrations used capsules as protective carriers for fluorescent/phosphorescent indicators for oxygen, ions,[30] etc. This has been followed by many similar sensors and a broad set of example applications, particularly for biological monitoring of cells in culture[31−35] and even some uses in whole organisms as indicators of, for example, stress.[36] The early visions of microcapsule sensors also included the possibilities for more complex protein-based sensing systems; these have been further developed into well-understood bioreactor-based systems such as enzymatic sensors[28,37−49] and encapsulated competitive-binding assays.[50−53] However, these examples have relied on microscale materials—in some cases, the larger size is essential for desired function,[44] whereas in other cases such as cellular analysis it would be advantageous to produce nanoscale particles that can penetrate smaller spaces and distribute more quickly.

As noted, prior work has employed various matrices for encapsulating sensing chemistry. However, there is no question that that the calcium carbonate-mediated approach is most popular and seems best-suited for use with more sensitive components such as enzymes and binding proteins because of the facile synthesis, high encapsulation efficiency, and mild dissolution requirements.[25,54] Taking advantage of the LbL approach and the template-based method, nanosized capsules have been reported.[22,23] These make use of solid nanoparticles other than nanosized vaterite $CaCO_3$, and therefore the encapsulation possibilities are limited to either surface adsorption prior to LbL or loading of cargo after creation of the LbL shell. However, recently a new approach was developed to fabricate nanosized porous vaterite $CaCO_3$ that remain stable over time when suspended in solution. Nagaraja et al.[55] developed a technique to fabricate calcium carbonate nanoparticles (CCNPs) utilizing PVSA. The addition of this polymer in the synthesis process serves to lower the nucleation rate and stabilize the surface to prevent further growth or aggregation into microparticles.

In this study, we explored the use of PVSA-stabilized vaterite CCNPs as templates for fabricating nanosized polymeric capsules. We examined the conditions for LbL deposition on the CCNPs stability and selected a preferred buffer system to be used for the LbL process. Using the template-based method in conjunction with the LbL approach, we studied the potential to encapsulate useful materials such as reporter dyes and nanoparticles. We investigated the effect encapsulated cargo has on the CCNPs size, and the effect varying concentrations of PVSA has on the cargo encapsulation efficiency. Finally, we used these findings to fabricate nanosized ratiometric oxygen sensors and evaluated the response at different dissolved oxygen concentrations.

EXPERIMENTAL SECTION

Chemicals. Poly(vinylsulfonic acid) (PVSA), sodium carbonate (Na_2CO_3), calcium chloride ($CaCl_2$), poly(sodium 4-styrenesulfonate) (PSS, average M_w 70 000 Da), poly(diallyldimethylammonium chloride) (PDADMAC, average M_w 100 000−200 000 Da), 2,2-dimethoxy-2-phenyl-acetophenone (Irgacure 651), ethylene glycol, ethylenediaminetetraacetic acid (EDTA), and buffer salts ($NaHCO_3$, CHES and TRIS) were obtained from Sigma and used as received. A 10 mM solution of Pd-meso-tetra(4-carboxyphenyl) porphine (PdTCPP, Frontier Scientific) in DMSO and a 2% suspension of 0.02 μm, yellow-green (505/515) carboxylate modified FluoSpheres (FS, Life Technologies) were used for all experiments. To fabricate hydrogels, we purchased tetraethylene glycol dimethacrylate (TEGDMA) and 2-hydroxyethyl methacrylate (HEMA) from Polysciences, Inc. (Warrington, PA, USA).

Nanoparticle Synthesis. A 10 mL solution of 20 mM $CaCl_2$ with PVSA was mixed under continuous stirring (800 rpm) in a 100 mL beaker with a wedge stir bar (VWR). The concentration of PVSA added was varied (0.62, 0.31, and 0.16 μM) to assess the effect of the polymer concentration on particle formation. After 5 min, 10 mL of 20 mM Na_2CO_3 was added rapidly and the beaker was covered while the reaction was allowed to occur for 4 h at 5 °C. All nucleation reactions were carried out at 5 °C, as monodisperse CCNPs with a fairly narrow size distribution are easily obtained at lower temperatures.[55] The mixture was then centrifuged at 7000 g for 15 min to recover formed CCNPs and remove excess reactants. The recovered CCNPs were washed three times in a rinse buffer of 0.1 M $NaHCO_3$ (pH 9). After washing, the particles were resuspended in 1 mL of the bicarbonate rinse buffer.

Encapsulation. The coprecipitation method[56] was employed to prepare cargo containing CCNPs. This is a modification of the protocol described above for nanoparticle synthesis with slight alterations to encapsulate the cargo of interest. Specifically, 200 μL of loading material (FS or/and PdTCPP) was added to 10 mL of 20 mM $CaCl_2$ containing PVSA (0.62 μM, 0.31 μM, 0.16 μM) under continuous stirring. The cargo-containing CCNPs were then washed in buffer to remove nonencapsulated cargo.

Encapsulation efficiency of FS was evaluated under three different concentrations of PVSA (0.62 μM, 0.31 μM, 0.16 μM) keeping the concentration of the FS constant at 0.78 nM. The fabricated CCNPs were washed in 0.1 M $NaHCO_3$ pH 9.0 buffer twice to remove nonencapsulated FS. Similar loading experiments were carried out to find the change in loading efficiency of PdTCPP with changing PVSA concentrations, when a constant concentration (194 μM) of PdTCPP was used.

To quantify encapsulation efficiency, we exposed particles to excess EDTA to release the encapsulated cargo. The concentration of the released FS was calculated by measuring the fluorescence at 515 nm when excited at 505 nm and using a predetermined calibration curve (see the Supporting Information, Figure S1) obtained from known concentrations of FS. Similarly, the concentration of PdTCPP released from CCNPs was determined by measuring the absorbance at 405 nm and using a calibration curve (see the Supporting Information, Figure S2). Encapsulation efficiency was calculated by comparing the concentration of cargo released after CCNP dissolution to the original concentration of cargo added during coprecipitation.

LbL Deposition of PEMs on the CaCO3 Nanoparticles (CCNPs). Using layer-by-layer (LbL) assembly, we deposited polyelectrolyte multilayers (PEMs) on the CCNPs (Scheme 1).

Scheme 1. Representation of Nanocapsule Formation via LbL Approach: (a) PVSA-Stabilized Vaterite CCNPs, (b) $[PDADMAC/PSS]_1$-Coated CCNPs, (c) $[PDADMAC/PSS]_{10}$-Coated CCNPs, (d) NCs with Ten Bilayers after Dissolution of $CaCO_3$ Core

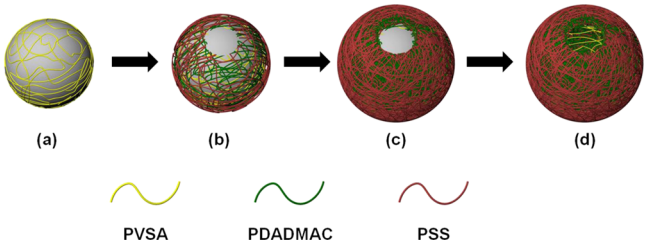

Briefly, CCNPs suspended in 1 mL of 0.1 M $NaHCO_3$ buffer (pH 9) were added dropwise to polyelectrolyte solutions subjected to constant sonication for 10 min. The polyelectrolytes employed were PDADMAC and PSS, each prepared at 20 mg/mL in 0.1 M $NaHCO_3$. The CCNPs were rinsed with 0.1 M $NaHCO_3$ pH 9 buffer between each deposition step to remove excess polyelectrolyte. PDADMAC was deposited initially followed by PSS/PDADAMAC until 10 bilayers were achieved. Hollow capsules were produced from the final PEM-coated CCNPs by exposing them to excess EDTA at pH 7.2.

Immobilization of Nanocapsules in Hydogels. Capsules were embedded in a hydrogel matrix for testing as a "pseudo solid-state" device. Briefly, 2.5 mg of Irgacure 651 and 90 μL of ethylene glycol were added to a polymer precursor solution containing 2-hydroxyethyl methacrylate (HEMA) and triethylene glycol-dimethacrylate (TEGDMA) in the molar ratio 49:1. A 100 μL aliquot of nanocapsule suspension in 0.1 M $NaHCO_3$ was added to the mixture of Irgacure, ethylene glycol and HEMA precursor and the final prepolymer was placed between two clean glass slides with a 0.03" Teflon spacer. The gel precursors were then photopolymerized by exposure to UV light (457 nm) (Ultra-Violet Products Ltd.) for 3 min on both sides.

Sensor Response Testing. The dissolved oxygen concentration in a reservoir containing 0.2 M PBS buffer (pH 7.2) was controlled by mixing air and nitrogen with mass flow controllers (type 1179A, MKS). The concentration of dissolved oxygen in the PBS buffer was determined with an oxygen microelectrode (PA2000, Unisense). Hydrogels affixed on glass slides were placed in a custom-made flow-through system and were exposed to PBS buffer containing different dissolved oxygen concentrations. To measure luminescence intensity, an ISS PC1 spectrofluorometer with a bifurcated fiber optic bundle attachment was used.

Characterization. All zeta potential measurements were performed using a Zeta Sizer Nano Series ZEN 3600 Spectrometer (Malvern Instruments Ltd., Malvern, Worcestershire, United Kingdom). For all measurements, 1/1000 diluted stock in 5 mM pH 9 $NaHCO_3$ buffer was used. A NanoSight LM10HS with a 65 mW 405 nm light source was used to determine particle size and size distributions. The sample stock was diluted 1/200 in 0.1 M pH 9 $NaHCO_3$ buffer and used for all measurements. A Hamamatsu C11440 digital camera was used to capture at least 1000 particle tracking events, which was then analyzed using NanoSight 2.3 software.

For all UV−VIS absorbance measurements a Cary 300 UV−VIS spectrophotometer with a 6 × 6 multicell Peltier block and temperature controller was used. All nucleation events were first scaled down to about 3 mL total reactant volume and absorbance at 500 nm was measured every 20−30 s to determine time required for nucleation and growth completion of the nanoparticles and also to detect for anomalies in nanoparticle growth profile.

Images of particle and capsules were captured using a JEOL 7500 scanning electron microscope with field emission source (FE-SEM) at the Texas A&M Materials Characterization Facility (MCF). Stock solutions of CCNPs/NCs were diluted to 1/20 and 2 μL of the diluted solution was placed on a clean silica support and dried in a vacuum chamber overnight. All samples were sputter-coated with 4 nm of palladium/platinum prior to taking the images. All EDS spectrum were obtained using an Oxford energy-dispersive X-ray spectrometry (EDS) system attached to the SEM system. SEM images were analyzed using ImageJ 1.48v software.

RESULTS

The electrostatic LbL approach to deposit PEMs on colloids involves alternate suspension of the colloidal particles in oppositely charged polyelectrolyte solutions, accompanied by rinsing steps in between each polyelectrolyte deposition step (Scheme 1). The buffer used for successfully coating CCNPs with PEMs without dissolving/altering the particles is critical, as the LbL process entails repeated cycles of washing and resuspension of the CCNPs. Therefore, the first step in developing this process was to understand the influence of buffer on coating and particle stability.

PVSA-stabilized vaterite CCNPs were fabricated according to the method described by Nagaraja et al.[55] It has been reported that vaterite CCNPs are more stable in alkaline conditions,[57] but we observed that the type of buffer used has an effect on CCNP stability as well. The CCNPs were not stable in all buffer systems at alkaline pH, for example, the CCNPs formed aggregates when suspended in alkaline phosphate buffer. We chose a moderately high pH, as depositing PEMs in extreme alkaline conditions would potentially have an adverse effect on any cargo encapsulated in or adsorbed on the CCNPs. The polyelectrolytes PDADMAC and PSS were chosen because they remain sufficiently charged at alkaline pH. The stability of the particles was analyzed for three different buffer systems (CHES, TRIS and $NaHCO_3$) keeping the pH constant at 9. For these studies, the fabrication process of the CCNPS was scaled down by adding 1.5 mL of 20 mM Na_2CO_3 to a stirred solution of 1.5 mL of 20 mM $CaCl_2$ containing 0.16 μM PVSA. The formed CCNPs were suspended in 5 mL of buffer and washed under sonication. This process was repeated six times. The CCNPs were washed repeatedly in buffer solutions to imitate the repeated cycles of washing and resuspension characteristic of the LbL process. The size distribution and concentration of the CCNPs were measured before and after washing (under sonication) in the three buffer systems (Figure 1). It was evident that CCNPs (mean diameter 170 nm) suspended in 0.1 M $NaHCO_3$ buffer pH 9.0 had greater concentration both before and after repeated washing in buffer, when compared to CCNPs suspended in 0.1 M CHES buffer (pH 9.0) and 0.1 M TRIS buffer (pH 9.0). Cumulative concentration of CCNPs suspended in $NaHCO_3$ before repeated washing was 637% and 249% greater than the cumulative concentration of CCNPs suspended in CHES and TRIS respectively. Insignificant decrease in particle concentration after washing the particles repeatedly in $NaHCO_3$ was also observed (Figure 1 inset).

Having established that the CCNPs are most stable in 0.1 M $NaHCO_3$ pH 9.0 buffer, the polyelectrolytes PDADMAC/PSS were suspended in 0.1 M $NaHCO_3$ pH 9.0 buffer and 0.1 M $NaHCO_3$ pH 9.0 buffer was used in all the rinsing steps of the LbL process. PEMs were deposited on CCNPs (mean dia.170 nm) using the method described earlier (Scheme 1). The zeta potential for the CCNPs was measured after each polyelec-

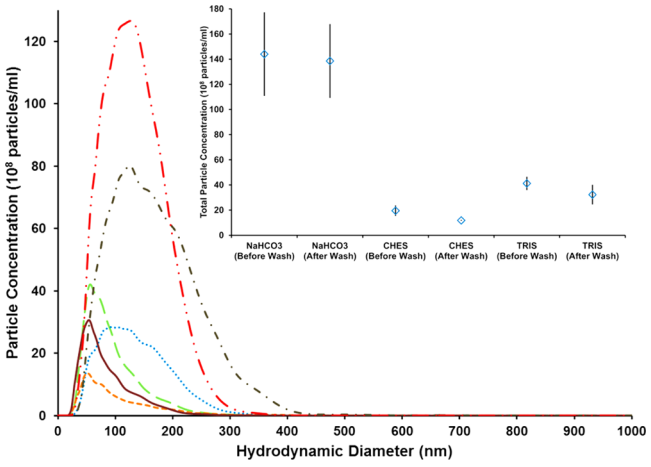

Figure 1. NTA plots showing the change in concentration of CCNPs before washing in $NaHCO_3$ (red dash-dot line), CHES (maroon solid line), TRIS (blue dotted line), and after washing in $NaHCO_3$ (black dash-dot line), CHES (orange dashed line), TRIS (green dashed line). Inset: Data representing cumulative concentration of CCNPs before and after washing in $NaHCO_3$, CHES, and TRIS buffer. Error bars represent 95% confidence intervals for three separate batches.

trolyte deposition step to confirm surface charge reversal. The results reported in Figure 2 show the zeta potential reversal

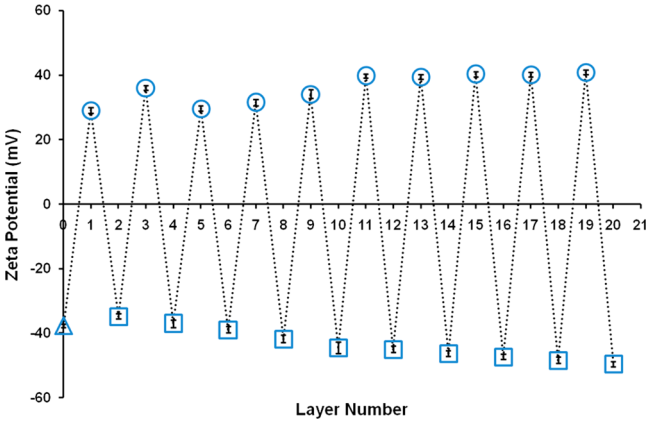

Figure 2. Zeta potential change with increase in the number of polymer layers coated on CCNPs. Δ = CCNP, ○ = PDADMAC, and □ =PSS. Error bars represent 95% confidence intervals for three separate batches.

after each deposition step of the cationic/anionic polyelectrolyte. The magnitude of the surface charge for the cationic and anionic polyelectrolyte-coated CCNPs is large (36.15 ± 4.70 mV; −43.31 ± 5.01 mV), suggesting colloidal stability of the suspended polyelectrolyte coated CCNPs. The zeta potential progressively increases in magnitude, revealing more complete polyelectrolyte coating with the increase in the number of polyelectrolyte layers that is commonly seen in PEM systems applied to small particulates. After the deposition of 10 bilayers, the PEM-coated CCNPs were well-dispersed when suspended in 0.1 M $NaHCO_3$ pH 9.0 buffer.

Hollow NCs were made using the process described earlier. The morphology of the CCNPs and the NCs was visualized by SEM imaging (Figure 3). The images of the CCNPs show a spherical morphology, which is typical for vaterite $CaCO_3$ particles. The SEM images of the NCs are similar to SEM images of microspheres consisting of a mixed population of spherical NCs and collapsed NCs.[58] This is expected, as dried capsules collapse during imaging, revealing folds and crevices because of their hollow interior. The average increase in diameter of colloidal particles coated with PDADMAC/PSS has been reported to be 5 nm per bilayer.[17] Comparing the diameters of the nanocapsules and the CCNPs we found an average increase of 33.6 nm with each bilayer of PDADMAC/PSS added. The unusual increase in the nanocapsule wall thickness may be attributed to the highly porous structure of the CCNPs, which favors the formation of thicker capsule walls, which has been observed in case of microcapsules fabricated from calcium carbonate microparticle templates as well.[1] Elemental analysis under higher magnification was carried out using an EDS system attached to the SEM to confirm that $CaCO_3$ was no longer present in the NCs. The EDS spectrum (Figure 4A) of the CCNPs shows a distinct calcium peak that is absent in the EDS spectrum of the NCs (Figure 4B). Both of the EDS spectra indicate the presence of platinum, palladium, and silicon resulting from the silicon substrate and the sputter-coated film.

To fabricate a ratiometric oxygen sensor, we chose Pd-meso-tetra (4-carboxyphenyl) porphine (PdTCPP), an oxygen sensitive phosphorescent dye, and carboxylate-modified FluoSpheres, which are not sensitive to oxygen, as the cargo to be entrapped in the polymeric nanocapsules. This combination of materials has overlapping excitation spectra and complementary emission spectra that allow for generation of a dual-peak emission using a single light source. Additionally, they represent two different model materials: dye molecules with poor water solubility and colloidally stable particles of a smaller size than the desired nanocapsules. Before preparation of NCs containing PdTCPP/FS, a series of experiments were performed to determine the effect of loading conditions on the encapsulation of PdTCPP and FS. As such, cargo-containing CCNPs were synthesized following the protocol described above with varying PVSA concentrations.

The results reported in Figure 5A show the loading efficiency of the FS when using different PVSA concentrations. The loading efficiency is almost unchanged when using 0.62 μM and 0.31 μM PVSA but reduces by almost 50% when 0.16 μM PVSA is used. The slight variations in size of the FS-loaded CCNPs with changing PVSA concentration is reported in Figure 5B.

Conversely, the PdTCPP encapsulation efficiency decreases by more than 50% from ∼12% to ∼5% when 0.62 μM PVSA is used instead of 0.31 μM PVSA. Keeping in mind our objective to maximize PdTCPP and FS loading efficiency, 0.16 μM PVSA concentration was not used as it yielded low FS encapsulation efficiency. Figure 5D shows the variation in size distribution of the PdTCPP loaded CCNPs with different PVSA concentrations. Size distribution of unloaded CCNPs with varying PVSA concentrations were also measured as a reference. From the loading experiments, it was evident that, of the concentrations tested, 0.31 μM PVSA was best suited to attain high loading of both encapsulates without significantly changing the size of the CCNPs.

Having identified a concentration of PVSA suitable for efficient loading of FS and PdTCPP, CCNPs containing both PdTCPP and FS were fabricated. CCNPs were coprecipitated with 0.31 μM PVSA, 194 μM PdTCPP and 0.78 nM of FS, and the cargo encapsulation efficiency was determined. The data reported in Figure 6 show the amount of FS and PdTCPP

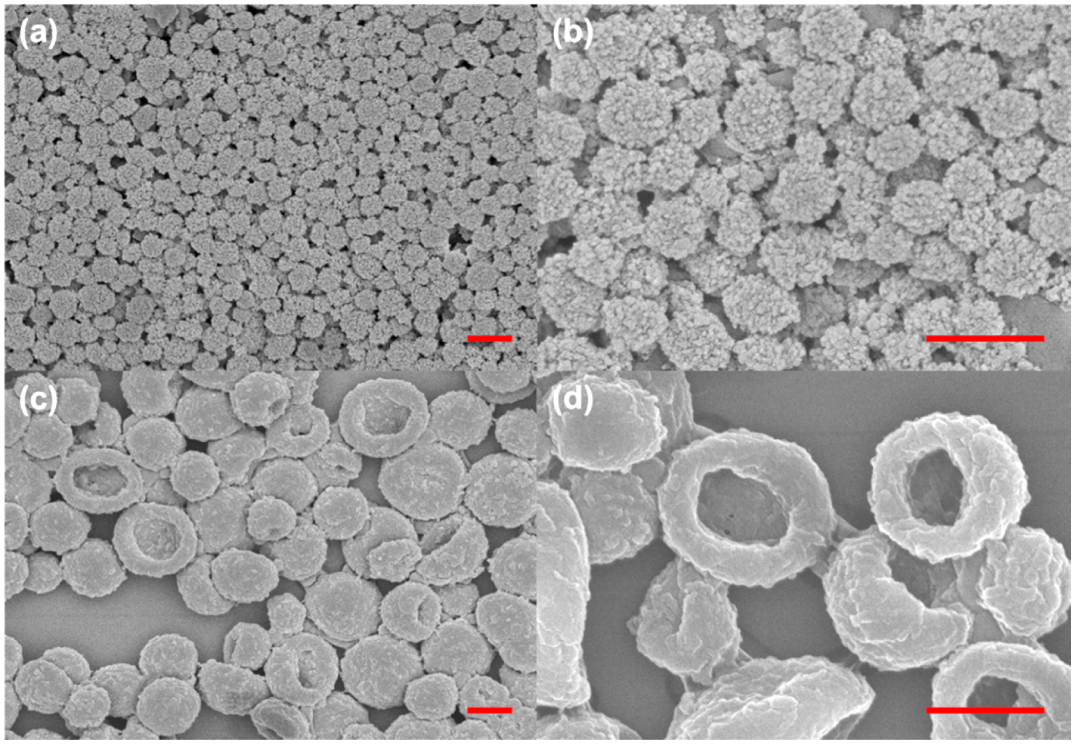

Figure 3. SEM images of sputter-coated CCNPs at (a) 20 000× magnification (b) 50 000× magnification and NCs at (c) 20 000× magnification and (d) 50 000× magnification. Scale bars correspond to 500 nm.

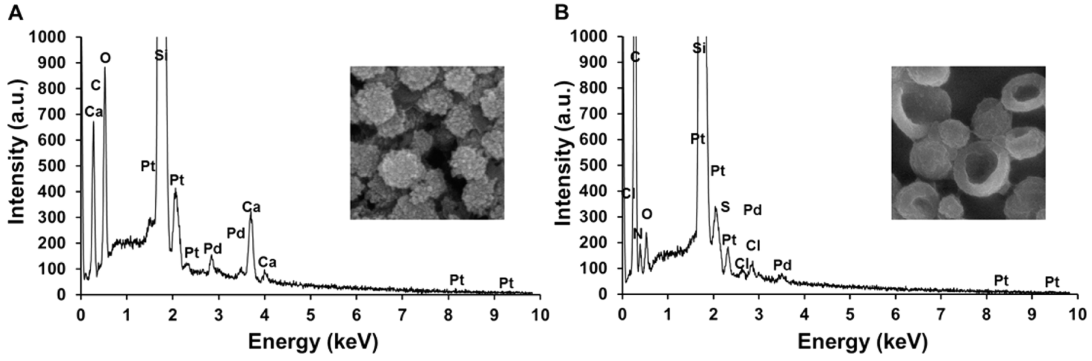

Figure 4. Energy-dispersive X-ray spectroscopy (EDS) spectra for sputter-coated (A) CCNPs and (B) NCs.

released from the CCNPs containing both FS and PdTCPP and is compared to the amount of FS/PdTCPP released from CCNPs containing only FS or PdTCPP. At least in this limited experiment, no significant difference was observed for either component FS or PdTCPP when both are encapsulated together compared to the individual cases. Therefore, it was determined appropriate to proceed with studying the sensor properties of NCs containing both PdTCPP and FS. Changes in loading efficiency with varying PVSA concentration and cargo content are tabulated in Table S1 (see the Supporting Information).

Using the conditions that favor maximum encapsulation of PdTCPP and FS, we fabricated NCs with 10 bilayers. The NCs containing both FS and PdTCPP would potentially function as ratiometric oxygen sensors (Scheme 2). To evaluate sensor response, we exposed the nanocapsules to buffer solutions having different concentrations of dissolved oxygen. We used a custom flow cell to expose the NCs to buffer solutions containing different oxygen levels. This required the NCs be immobilized in the flow chamber. Trapping the NCs in a hydrogel and affixing the hydrogel in the flow chamber allowed for a larger volume of NCs to be suspended and interrogated in a 3D gel, generating a larger signal for improved SNR. This approach was also more practical than affixing the NCs directly to the glass slide in a single layer.

The data reported in Figure 7 shows the normalized emission intensity spectrum of the NCs containing pHEMA slabs when excited at 405 nm while exposed to different oxygen concentrations. The photon counts at 700 nm gradually increased when the oxygen concentration was decreased in steps from 243.7 to 0 μM, whereas the photon counts at 515 nm remains constant. The decreased photon count at higher oxygen concentrations is due to the quenching effect molecular oxygen has on the PdTCPP dye.

A plot of the counts ratio R (counts @ 700 nm/counts @ 515 nm) shows that the response of the nanosensors is more linear in the lower oxygen concentrations than in the higher oxygen concentrations (Figure 8). The profile is well-matched

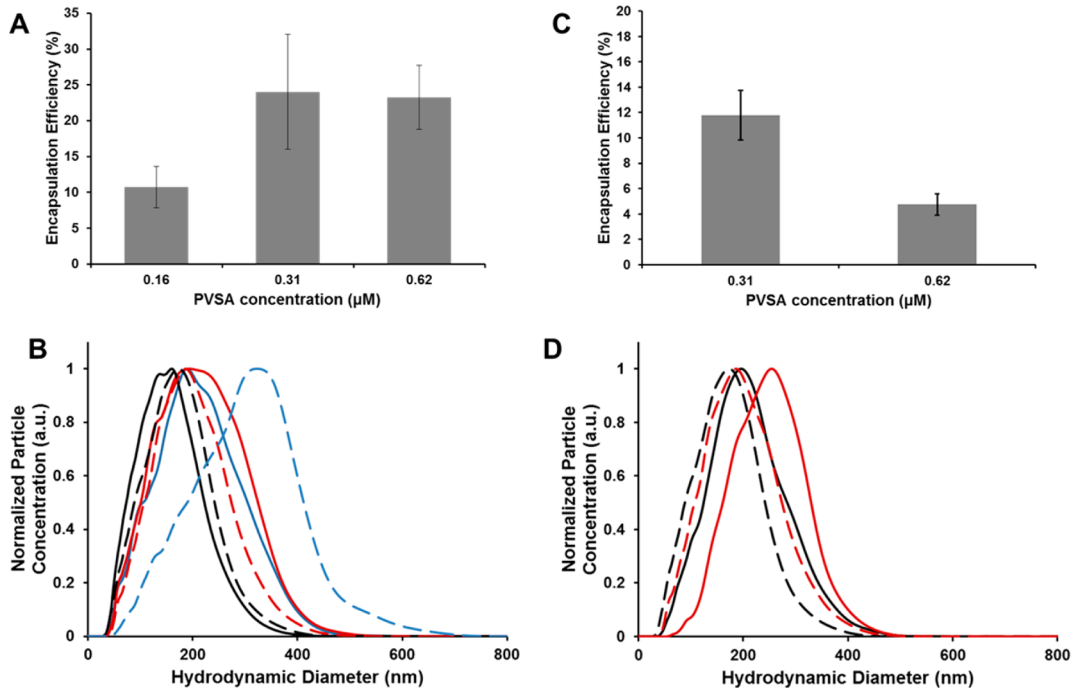

Figure 5. (A) Encapsulation efficiency of FS in CCNPs at different PVSA concentrations. Error bars represent 95% confidence intervals for three separate batches of CCNPs. (B) Size distribution of FS-loaded CCNPs at 0.16 μM (blue solid line), 0.31 μM (red solid line), and 0.62 μM (black solid line) PVSA, compared to size distribution of unloaded CCNPs at 0.16 μM (blue dashed line), 0.31 μM (red dashed line), and 0.62 μM (black dashed line) PVSA. (C) Encapsulation efficiency of PdTCPP in CCNPs at different PVSA concentrations. Error bars represent 95% confidence intervals for three separate batches of CCNPs. (D) Size distribution of PdTCPP loaded CCNPs at 0.31 μM (red solid line) and 0.62 μM, (black solid line) PVSA, compared to size distribution of unloaded CCNPs at 0.31 μM (red dashed line) and 0.62 μM, (black dashed line) PVSA.

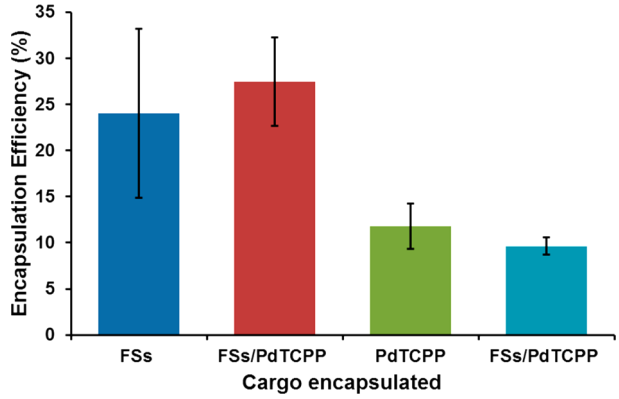

Figure 6. Data representing encapsulation efficiency of FS in FS (0.78 nM) loaded CCNPs (blue), (0.78 nM) FS/ (194 μM) PdTCPP loaded CCNPs (red), and encapsulation efficiency of PdTCPP in PdTCPP (194 μM) loaded CCNPs (green), (0.78 nM) FS/(194 μM) PdTCPP loaded CCNPs (light blue). Error bars represent 95% confidence intervals for three separate batches of CCNPs.

to a second-order exponential curve (R^2 = 0.999), and was used to calculate the range and the average sensitivity of the nanosensors. The limit of detection (LOD) was calculated by interpolating $R_{700/515.max} - 3\sigma$ on the curve, and the maximum differentiable oxygen concentration (MDOC) was calculated by interpolating $R_{700/515.min} + 3\sigma$ on the curve, where σ denotes the standard deviation of the ratio (a measure of signal variability). From the calculated values of LOD = 7.62 μM and MDOC = 139.31 μM, the range was calculated as MDOC-LOD = 131.69 μM. It has been well-documented that hypoxic conditions prevails at tumor sites (median partial pressure O_2 < 10 mm of Hg).[59,60] Using Henry's gas law, the LOD of the NCs was estimated to be 4.45 mm of Hg, making them potential candidates for use in monitoring oxygen levels at tumor sites. The quenching sensitivity Q was calculated using $[(R_{min} - R_{max})/R_{min}]\cdot 100$, where R_{min} denotes the 700 nm/515 nm intensity ratio at 0 μM oxygen concentration and R_{max} denotes the 700 nm/515 nm intensity ratio at 243.7 μM oxygen concentration. The quenching sensitivity Q was determined to be 89.28 $\pm$ 2.59%. Average sensor sensitivity was calculated using the formula $S = Q/(\text{MDOC-LOD})$. For the three different sensors we tested, the average sensitivity was found to be 0.68 $\pm$ 0.02% change/μM oxygen. The oxygen concentration level at which the sensor is best suited to operate[61] may be defined by O_2 (S = 1/2), the oxygen concentration at $R_{700/515.max}$ / 2. Calculations revealed O_2 (S = 1/2) to be 20.91 μM of dissolved oxygen.

Using the Stern–Volmer equation $I_0/I = 1 + K_{SV}[O_2]$, I_0/I (intensity at 700 nm) was plotted against the oxygen concentration (Figure 8 inset), which gives a K_{SV} value of 0.05 μM^{-1}. It is evident that at higher oxygen concentrations there is decreased linearity in the S–V curve, the downward curvature may be explained by unequal access to the dye by oxygen,[62] and by the presence of nonhomogeneous microenvironments surrounding the dye molecules.[63]

Different strategies have been explored to fabricate oxygen sensitive probes[64] utilizing metallo-organic complexes,[63,65] organic dyes[66] and nanoparticles.[67] In comparison to organic dyes, metallo-organic complexes have stronger luminescent quenching properties, making them more desirable for sensing purposes. In the presence of molecular oxygen, excited metallo-organic complexes transfer energy to the molecular oxygen present, subsequently returning to the ground state without emitting any photon. Single intensity measurement luminescent

Scheme 2. Representation Showing the Cross-Sectional View of a Nanocapsule Containing FS and PdTCPP

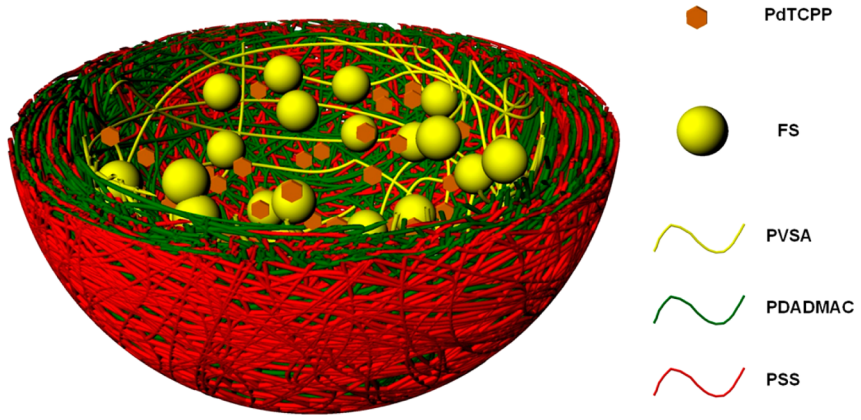

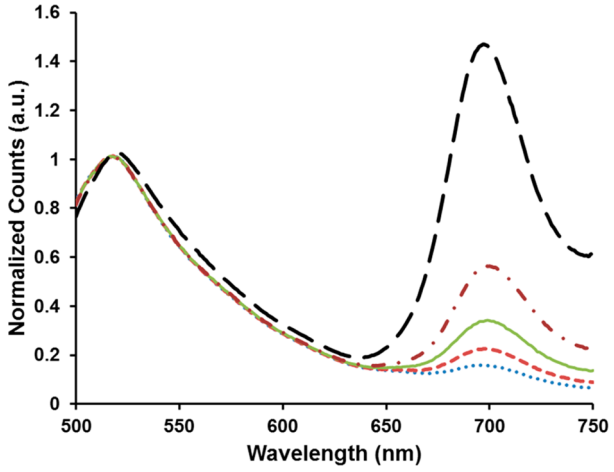

Figure 7. Emission spectra of NCs containing FS and PdTCPP immobilized in pHEMA hydrogels at 243.7 μM (blue dotted line), 121.9 μM (red dashed line), 60.9 μM (green solid line), 30.4 μM (maroon dash-dot line), and 0 μM (black dashed line) dissolved oxygen concentration when excited at 405 nm. Data represents the average spectrum of three different hydrogels.

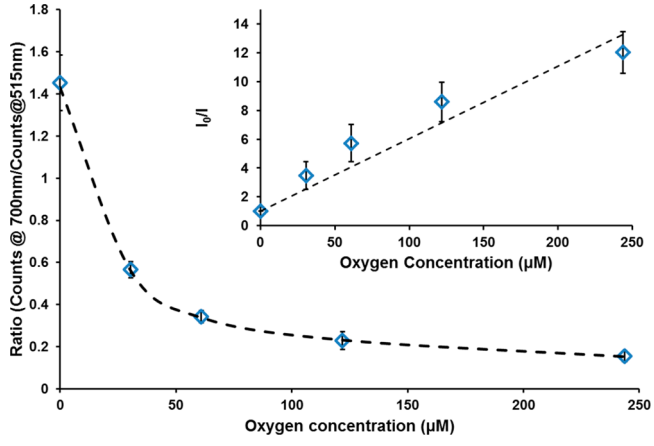

Figure 8. Plot of ratio (counts @ 700 nm/counts @ 515 nm) against increasing dissolved oxygen concentration. Error bars represent 95% confidence intervals for three separate batches of NCs containing hydrogels. Inset: Data representing change in I_0/I with increasing dissolved oxygen concentration. I_0 = intensity at 700 nm when dissolved oxygen concentration is 0 μM. Error bars represent 95% confidence intervals for three separate batches of NCs containing hydrogels.

sensors have certain innate drawbacks, such as variations in luminescent intensity with power fluctuations in excitation source and scattering from the sample. Incorporating a reference dye along with an oxygen sensitive dye alleviates the problems associated with single intensity measurements, by calculating the ratio of the indicator intensity and the reference intensity.[64] In our oxygen sensing NCs, we used oxygen sensitive PdTCPP as the indicator dye while using FS as the reference dye. The significant spectral difference between the luminescence and phosphorescence makes ratiometric intensity measurements facile. Ratiometric oxygen sensors employing similar palladium porphyrin dyes have been fabricated in the past and approximate quenching sensitivities of 57−88[68] and 72[69] have been reported, which compares well to the quenching sensitivity of our sensor.

CONCLUSION

In this work, we show the procedure development for the fabrication of oxygen sensitive polymer nanocapsules via the LbL approach using vaterite CCNPs as sacrificial templates. We found that the buffer type plays a crucial role in maintaining the CCNP integrity throughout the LbL process, finding that CCNPs were most stable in alkaline $NaHCO_3$. By varying the PVSA concentration during coprecipitation with sensor components we found a trade-off between encapsulation efficiency and nanoparticle size. We found that by decreasing PVSA concentration we could improve encapsulation of PdTCPP without a substantial increase in CCNP size. The constructed oxygen sensitive nanocapsules were evaluated in a flow through system and were found to have a limit of detection and maximum differentiable oxygen concentration of 7.62 and 139.31 μM of dissolved oxygen, respectively, giving us an analytical range of 131.69 μM of dissolved oxygen. The quenching sensitivity and O_2 (S = 1/2) were calculated to be 89.28 ± 2.59% and 20.91 μM of dissolved oxygen, respectively.

We expect that the nanocapsule properties could be easily tuned for other applications by selecting the appropriate polyelectrolytes. However, the pH and buffer considerations required to maintain CCNP integrity limits the conditions and polyelectrolytes that can be used for the first several bilayers. We speculate that by altering the payload contained in the nanocapsules, such nanocapsules will find other uses in the field of sensing, drug delivery, and catalysis. Our future work will be focused on exploring the use of other polyelectrolytes to

fabricate nanocapsules with effective diffusion barrier in order to investigate the use of the ratiometric oxygen sensors in vivo.

■ ASSOCIATED CONTENT

Supporting Information

Additional table and figures. This material is available free of charge via the Internet at http://pubs.acs.org.

■ AUTHOR INFORMATION

Corresponding Author

*E-mail: mcshane@tamu.edu. Phone: 979-845-7941. Fax: 979-845-4450 .

Author Contributions

The manuscript was written through contributions of all authors. All authors have given approval to the final version of the manuscript.

Funding

This research was supported by the National Science Foundation under Grants 1066928 and 1258696.

Notes

The authors declare no competing financial interest.

■ ACKNOWLEDGMENTS

We thank Yil-Hwan You for his insight and expertise in SEM imaging. Use of the TAMU Materials Characterization Facility is acknowledged.

■ REFERENCES

(1) Volodkin, D. V.; Petrov, A. I.; Prevot, M.; Sukhorukov, G. B. Matrix Polyelectrolyte Microcapsules: New System for Macromolecule Encapsulation. *Langmuir* **2004**, *20*, 3398−3406.

(2) Mora-Huertas, C. E.; Fessi, H.; Elaissari, A. Polymer-based nanocapsules for drug delivery. *Int. J. Pharm.* **2010**, *385*, 113−142.

(3) He, C.; Hu, Y.; Yin, L.; Tang, C.; Yin, C. Effects of particle size and surface charge on cellular uptake and biodistribution of polymeric nanoparticles. *Biomaterials* **2010**, *31*, 3657−3666.

(4) Shubayev, V. I.; Pisanic Ii, T. R.; Jin, S. Magnetic nanoparticles for theragnostics. *Adv. Drug Delivery Rev.* **2009**, *61*, 467−477.

(5) Maeda, H. Tumor-Selective Delivery of Macromolecular Drugs via the EPR Effect: Background and Future Prospects. *Bioconjugate Chem.* **2010**, *21*, 797−802.

(6) Hobbs, S. K.; Monsky, W. L.; Yuan, F.; Roberts, W. G.; Griffith, L.; Torchilin, V. P.; Jain, R. K. Regulation of transport pathways in tumor vessels: Role of tumor type and microenvironment. *Proc. Natl. Acad. Sci. U.S.A.* **1998**, *95*, 4607−4612.

(7) Evans, S. M.; Koch, C. J. Prognostic significance of tumor oxygenation in humans. *Cancer Lett.* **2003**, *195*, 1−16.

(8) Warburg, O. On the Origin of Cancer Cells. *Science* **1956**, *123*, 309−314.

(9) Izumi, H.; Torigoe, T.; Ishiguchi, H.; Uramoto, H.; Yoshida, Y.; Tanabe, M.; Ise, T.; Murakami, T.; Yoshida, T.; Nomoto, M.; Kohno, K. Cellular pH regulators: potentially promising molecular targets for cancer chemotherapy. *Cancer Treat. Rev.* **2003**, *29*, 541−549.

(10) O'Brien, D. F.; Armitage, B.; Benedicto, A.; Bennett, D. E.; Lamparski, H. G.; Lee, Y.-S.; Srisiri, W.; Sisson, T. M. Polymerization of Preformed Self-Organized Assemblies. *Acc. Chem. Res.* **1998**, *31*, 861−868.

(11) Zhang, L.; Eisenberg, A. Multiple Morphologies of "Crew-Cut" Aggregates of Polystyrene-b-poly(acrylic acid) Block Copolymers. *Science* **1995**, *268*, 1728−1731.

(12) Cui, J.; van Koeverden, M. P.; Müllner, M.; Kempe, K.; Caruso, F. Emerging methods for the fabrication of polymer capsules. *Adv. Colloid Interface Sci.* **2014**, *207*, 14−31.

(13) Huang, X.; Voit, B. Progress on multi-compartment polymeric capsules. *Polym. Chem.* **2013**, *4*, 435−443.

(14) Meier, W. Polymer nanocapsules. *Chem. Soc. Rev.* **2000**, *29*, 295−303.

(15) Sarti, S.; Bordi, F. Polymeric hollow micro and nanospheres for biotechnological applications: A focused review. *Mater. Lett.* **2013**, *109*, 134−139.

(16) Decher, G. Fuzzy Nanoassemblies: Toward Layered Polymeric Multicomposites. *Science* **1997**, *277*, 1232−1237.

(17) Sukhorukov, G. B.; Donath, E.; Lichtenfeld, H.; Knippel, E.; Knippel, M.; Budde, A.; Möhwald, H. Layer-by-layer self assembly of polyelectrolytes on colloidal particles. *Colloids Surf., A* **1998**, *137*, 253−266.

(18) Tong, W.; Song, X.; Gao, C. Layer-by-layer assembly of microcapsules and their biomedical applications. *Chem. Soc. Rev.* **2012**, *41*, 6103−6124.

(19) De Geest, B. G.; Sanders, N. N.; Sukhorukov, G. B.; Demeester, J.; De Smedt, S. C. Release mechanisms for polyelectrolyte capsules. *Chem. Soc. Rev.* **2007**, *36*, 636−649.

(20) Donath, E.; Sukhorukov, G. B.; Caruso, F.; Davis, S. A.; Möhwald, H. Novel Hollow Polymer Shells by Colloid-Templated Assembly of Polyelectrolytes. *Angew. Chem., Int. Ed.* **1998**, *37*, 2201−2205.

(21) Lee, D.; Rubner, M. F.; Cohen, R. E. Formation of Nanoparticle-Loaded Microcapsules Based on Hydrogen-Bonded Multilayers. *Chem. Mater.* **2005**, *17*, 1099−1105.

(22) Schuetz, P.; Caruso, F. Copper-Assisted Weak Polyelectrolyte Multilayer Formation on Microspheres and Subsequent Film Cross-linking. *Adv. Funct. Mater.* **2003**, *13*, 929−937.

(23) Marinakos, S. M.; Novak, J. P.; Brousseau, L. C.; House, A. B.; Edeki, E. M.; Feldhaus, J. C.; Feldheim, D. L. Gold Particles as Templates for the Synthesis of Hollow Polymer Capsules. Control of Capsule Dimensions and Guest Encapsulation. *J. Am. Chem. Soc.* **1999**, *121*, 8518−8522.

(24) Sukhorukov, G. B.; Volodkin, D. V.; Gunther, A. M.; Petrov, A. I.; Shenoy, D. B.; Mohwald, H. Porous calcium carbonate microparticles as templates for encapsulation of bioactive compounds. *J. Mater. Chem.* **2004**, *14*, 2073−2081.

(25) McShane, M.; Ritter, D. Microcapsules as optical biosensors. *J. Mater. Chem.* **2010**, *20*, 8189−8193.

(26) Duchesne, T. A.; Brown, J. Q.; Guice, K. B.; Lvov, Y. M.; McShane, M. J. Encapsulation and stability properties of nano-engineered polyelectrolyte capsules for use as fluorescent sensors. *Sens. Mater.* **2002**, *14*, 293−308.

(27) McShane, M. J., Nanoengineering of fluorescence-based chemical sensors using electrostatic self-assembly: Thin films and micro/nanoshells. In *Proceedings of the IEEE International Conference on Sensors 2002*; Orlando, June 12−14, 2002 ; IEEE: Piscataway, NJ, 2002; Vol. *1*, pp 293−297.

(28) McShane, M. J. Potential for glucose monitoring with nanoengineered fluorescent biosensors. *Diabetes Technol. Ther.* **2002**, *4*, 533−538.

(29) McShane, M. J.; Brown, J. Q.; Guice, K. B.; Lvov, Y. M. Polyelectrolyte microshells as carriers for fluorescent sensors: loading and sensing properties of a ruthenium-based oxygen indicator. *J. Nanosci. Nanotechnol.* **2002**, *2*, 411−416.

(30) Brown, J. Q.; McShane, M. J. Nanoengineered polyelectrolyte micro-and nano-capsules as fluorescent potassium ion sensors. *IEEE Eng. Med. Biol. Mag.* **2003**, *22*, 118−123.

(31) Kreft, O.; Javier, A. M.; Sukhorukov, G. B.; Parak, W. J. Polymer microcapsules as mobile local pH-sensors. *J. Mater. Chem.* **2007**, *17*, 4471−4476.

(32) Reibetanz, U.; Halozan, D.; Brumen, M.; Donath, E. Flow cytometry of HEK 293T cells interacting with polyelectrolyte multilayer capsules containing fluorescein-labeled poly (acrylic acid) as a pH sensor. *Biomacromolecules* **2007**, *8*, 1927−1933.

(33) Muñoz Javier, A.; Kreft, O.; Semmling, M.; Kempter, S.; Skirtach, A. G.; Bruns, O. T.; del Pino, P.; Bedard, M. F.; Rädler, J.; Käs, J. Uptake of Colloidal Polyelectrolyte-Coated Particles and Polyelectrolyte Multilayer Capsules by Living Cells. *Adv. Mater.* **2008**, *20*, 4281−4287.

(34) Kozlovskaya, V.; Kharlampieva, E.; Khanal, B. P.; Manna, P.; Zubarev, E. R.; Tsukruk, V. V. Ultrathin layer-by-layer hydrogels with incorporated gold nanorods as pH-sensitive optical materials. *Chem. Mater.* **2008**, *20*, 7474−7485.
(35) Rivera_Gil, P.; Nazarenus, M.; Ashraf, S.; Parak, W. J. pH-Sensitive Capsules as Intracellular Optical Reporters for Monitoring Lysosomal pH Changes Upon Stimulation. *Small* **2012**, *8*, 943−948.
(36) Sadovoy, A.; Teh, C.; Korzh, V.; Escobar, M.; Meglinski, I. Microencapsulated bio-markers for assessment of stress conditions in aquatic organisms in vivo. *Laser Phys. Lett.* **2012**, *9*, 542.
(37) Nayak, S. R.; Stein, E. W.; Gupta, N.; Palmer, J.; McShane, M. J. Transport of macromolecules through polyelectrolyte microcapsules -- Effect of molecular size and shell materials. In *Abstracts of Papers from the 226th ACS National Meeting*; New York, Sept 7−11, 2003 ; American Chemical Society: Washington, D.C., 2003; PMSE-204.
(38) Brown, J. Q.; McShane, M. J. Optimal design of nanoengineered implantable optical sensors using a genetic algorithm. In *Proceedings of the 26th Annual International Conference of the IEEE Engineering in Medicine and Biology Society*; San Francisco, Sept 1−4, 2004 ; IEEE, Piscataway, NJ, 2004; p 2105.
(39) Brown, J. Q.; Srivastava, R.; McShane, M. J. Encapsulation of glucose oxidase and an oxygen-quenched fluorophore in polyelectrolyte-coated calcium alginate microspheres as optical glucose sensor systems. *Biosens. Bioelectron.* **2005**, *21*, 212−216.
(40) Srivastava, R.; Brown, J. Q.; Zhu, H.; McShane, M. J. Stable encapsulation of active enzyme by application of multilayer nanofilm coatings to alginate microspheres. *Macromol. Biosci.* **2005**, *5*, 717−727.
(41) Stein, E. W.; McShane, M. J. Real-time temporal and spatial consumption of glucose within polyelectrolyte microspheres containing co-immobilized glucose oxidase and peroxidase. In *Abstracts of Papers from the 230th ACS National Meeting*; Washington, DC, Aug 28−Sept. 1, 2005 ; American Chemical Society: Washington, D.C., 2005; PMSE-353.
(42) Zhu, H.; McShane, M. J. Macromolecule encapsulation in diazoresin-based hollow polyelectrolyte microcapsules. *Langmuir* **2005**, *21*, 424−430.
(43) Zhu, H.; Srivastava, R.; Brown, J. Q.; McShane, M. J. Combined physical and chemical immobilization of glucose oxidase in alginate microspheres improves stability of encapsulation and activity. *Bioconjugate Chem.* **2005**, *16*, 1451−1458.
(44) Brown, J. Q.; McShane, M. J. Modeling of spherical fluorescent glucose microsensor systems: design of enzymatic smart tattoos. *Biosens Bioelectron* **2006**, *21*, 1760−1769.
(45) McShane, M. J., Microcapsules as "smart tattoo" glucose sensors: engineering systems with enzymes and glucose-binding sensing elements. In *Topics in Fluorescence Spectroscopy*; Geddes, C. D., Lakowicz, J. R., Eds. Springer: New York, 2006; Vol. *11*.
(46) Nayak, S. R.; McShane, M. J. Fluorescence glucose monitoring based on transduction of enzymatically-driven pH changes within microcapsules. *Sens. Lett.* **2006**, *4*, 433−439.
(47) Stein, E. W.; Volodkin, D. V.; McShane, M. J.; Sukhorukov, G. B. Real-time assessment of spatial and temporal coupled catalysis within polyelectrolyte microcapsules containing coimmobilized glucose oxidase and peroxidase. *Biomacromolecules* **2006**, *7*, 710−719.
(48) Singh, S.; McShane, M. Enhancing the longevity of microparticle-based glucose sensors towards 1 month continuous operation. *Biosens. Bioelectron.* **2010**, *25*, 1075−1081.
(49) McShane, M. J. Enzyme immobilization in polyelectrolyte microcapsules. *Methods Mol. Biol.* **2011**, *679*, 147−154.
(50) Chinnayelka, S.; McShane, M. J. Glucose-sensitive nanoassemblies comprising affinity-binding complexes trapped in fuzzy microshells. *J. Fluoresc.* **2004**, *14*, 585−595.
(51) Chinnayelka, S.; McShane, M. J. Microcapsule biosensors using competitive binding resonance energy transfer assays based on apoenzymes. *Anal. Chem.* **2005**, *77*, 5501−5511.
(52) Chinnayelka, S.; McShane, M. J. Glucose sensors based on microcapsules containing an orange/red competitive binding resonance energy transfer assay. *Diabetes Technol. Ther.* **2006**, *8*, 269−278.
(53) Chinnayelka, S.; Zhu, H.; McShane, M. Near-Infrared Resonance Energy Transfer Glucose Biosensors in Hybrid Microcapsule Carriers. *J. Sens.* **2008**, *2008*, No. 346016.
(54) Wang, Y.; Price, A. D.; Caruso, F. Nanoporous colloids: building blocks for a new generation of structured materials. *J. Mater. Chem.* **2009**, *19*, 6451−6464.
(55) Nagaraja, A. T.; Pradhan, S.; McShane, M. J. Poly (vinylsulfonic acid) assisted synthesis of aqueous solution stable vaterite calcium carbonate nanoparticles. *J. Colloid Interface Sci.* **2014**, *418*, 366−372.
(56) Petrov, A. I.; Volodkin, D. V.; Sukhorukov, G. B. Protein—Calcium Carbonate Coprecipitation: A Tool for Protein Encapsulation. *Biotechnol. Prog.* **2005**, *21*, 918−925.
(57) Chen, S.-F.; Colfen, H.; Antonietti, M.; Yu, S.-H. Ethanol assisted synthesis of pure and stable amorphous calcium carbonate nanoparticles. *Chem. Commun.* **2013**, *49*, 9564−9566.
(58) Volodkin, D. V.; Petrov, A. I.; Prevot, M.; Sukhorukov, G. B. Matrix polyelectrolyte microcapsules: new system for macromolecule encapsulation. *Langmuir* **2004**, *20*, 3398−3406.
(59) Höckel, M.; Vaupel, P. Tumor Hypoxia: Definitions and Current Clinical, Biologic, and Molecular Aspects. *J. Natl. Cancer Inst.* **2001**, *93*, 266−276.
(60) Höckel, M.; Schlenger, K.; Höckel, S.; Vaupel, P. Hypoxic Cervical Cancers with Low Apoptotic Index Are Highly Aggressive. *Cancer Res.* **1999**, *59*, 4525−4528.
(61) Mills, A. Controlling the sensitivity of optical oxygen sensors. *Sensors Actuators B: Chem.* **1998**, *51*, 60−68.
(62) Lakowicz, J. R. *Principles of Fluorescence Spectroscopy*; Springer: New York, 2007.
(63) Hartmann, P.; Leiner, M. J. P.; Lippitsch, M. E. Luminescence Quenching Behavior of an Oxygen Sensor Based on a Ru(II) Complex Dissolved in Polystyrene. *Anal. Chem.* **1995**, *67*, 88−93.
(64) Feng, Y.; Cheng, J.; Zhou, L.; Zhou, X.; Xiang, H. Ratiometric optical oxygen sensing: a review in respect of material design. *Analyst* **2012**, *137*, 4885−4901.
(65) Papkovsky, D. B.; Ponomarev, G. V.; Trettnak, W.; O'Leary, P. Phosphorescent Complexes of Porphyrin Ketones: Optical Properties and Application to Oxygen Sensing. *Anal. Chem.* **1995**, *67*, 4112−4117.
(66) Amao, Y.; Okura, I. Optical Oxygen Sensing Properties of Tris (4,7[prime]-diphenyl-1,10[prime]-phenanthroline) Ruthenium (II)-Polyacrylic Acid Complex Thin Film. *Polym. J.* **2000**, *32*, 452−455.
(67) Wu, C.; Bull, B.; Christensen, K.; McNeill, J. Ratiometric Single-Nanoparticle Oxygen Sensors for Biological Imaging. *Angew. Chem., Int. Ed.* **2009**, *48*, 2741−2745.
(68) Koo Lee, Y.-E.; Ulbrich, E. E.; Kim, G.; Hah, H.; Strollo, C.; Fan, W.; Gurjar, R.; Koo, S.; Kopelman, R. Near Infrared Luminescent Oxygen Nanosensors with Nanoparticle Matrix Tailored Sensitivity. *Anal. Chem.* **2010**, *82*, 8446−8455.
(69) Chu, C.-S.; Lo, Y.-L. Ratiometric fiber-optic oxygen sensors based on sol−gel matrix doped with metalloporphyrin and 7-amino-4-trifluoromethyl coumarin. *Sensors Actuators B: Chem.* **2008**, *134*, 711−717.